

Experimental Investigations for the Thermal Qualification of High Speed Missile Radomes

Oliver M. Hohn¹, Burkard Esser², Josef Klevanski³, Ali Gülhan⁴,
Resul Fener⁵, Britta Panthen⁶ and Martin Friess⁷

¹Supersonic and Hypersonic Technologies Department, German Aerospace Center (DLR)
Linder Höhe, 51147 Cologne, Germany, oliver.hohn@dlr.de

²Supersonic and Hypersonic Technologies Department, German Aerospace Center (DLR)
Linder Höhe, 51147 Cologne, Germany, burkard.esser@dlr.de

³Supersonic and Hypersonic Technologies Department, German Aerospace Center (DLR)
Linder Höhe, 51147 Cologne, Germany, josef.klevanski@dlr.de

⁴Supersonic and Hypersonic Technologies Department, German Aerospace Center (DLR)
Linder Höhe, 51147 Cologne, Germany, ali.guelhan@dlr.de

⁵Institute of Materials Research, German Aerospace Center (DLR)
Linder Höhe, 51147 Cologne, Germany, resul.fener@dlr.de

⁶Institute of Materials Research, German Aerospace Center (DLR)
Linder Höhe, 51147 Cologne, Germany, britta.panthen@dlr.de

⁷Institute of Structures and Design, German Aerospace Center (DLR)
Pfaffenwaldring 38-40, 70569 Stuttgart, Germany, martin.friess@dlr.de

Abstract

This paper presents the results of experimental investigations for the thermal qualification of radomes for high-speed missiles made of the oxide ceramic matrix composites WHIPOX and OXIPOL with different types of thermal insulation based on silica aerogels. Experiments were conducted in a blowdown windtunnel for aerothermodynamic investigations at Mach 3 flight conditions and in an arc-heated windtunnel at flight-relevant heat loads of higher Mach numbers derived from sample trajectories. Thermocouples and infrared thermography were used to measure the temperature distribution on the interior and exterior surfaces of the radome and the heating of a seeker head demonstrator.

1. Introduction

Ceramic matrix composites (CMC) are increasingly becoming the material of choice for thermally highly stressed components in aerospace applications. These materials offer a good compromise of high temperature stability (strength and stiffness) and low weight. For high speed air defence missiles thermal highly loaded components include radomes, control surfaces such as canards or fins and engine components like inlet ramps or nozzles.

In the present study, the use of two oxide CMCs for the use in radomes is investigated: WHIPOX (**w**ound **h**ighly **p**orous **o**xide CMC) [1, 2, 3, 4] and OXIPOL (**o**xide CMC based on **p**olymers) [5, 6, 7, 8]. While these materials use different fibres, Nextel 610 for WHIPOX and Nitivy for OXIPOL, and matrices (aluminium oxide for WHIPOX and SiOC for OXIPOL), the more important difference lie in their production methods. Both materials have been generally qualified in DLRs arc heated wind tunnel facilities for the use in high temperature applications with surface temperature beyond 1,700 K [9, 10]. The scope of the present investigation is to examine the suitability of the materials for the use as radomes not only regarding their own thermal behaviour but also concerning the heating of the seeker head that is covered by the radome. For the latter part, the possibility of thermal insulation of the radome based on silica aerogels is addressed as well. Three different types of thermal insulation are investigated in addition to a radome without insulation. The different test configurations are explained in section 2.2.

As the direct replication of flight conditions of a whole trajectory, especially with regard to occurring heat loads, of a high speed missile in ground testing facilities is not possible, a combined approach of different experimental and numerical examinations is used to verify the thermal suitability of these materials for the application in missile radomes. This paper presents the results of the experimental part of the investigation.

One part of the experimental examinations consist in direct testing at flight condition, which is possible in DLR's VMK facility up to certain limits (Mach 2.8 at sea level, Mach 3 in 4.5 km and Mach 3.2 in 7 km altitude, respectively). These testing capabilities are extensively used in the investigation. However, especially regarding flight Mach number and occurring heatloads, modern missile systems by far exceed these limits for significant parts of their trajectories which requires testing in hot windtunnel facilities that are able to replicate the higher heatloads of these trajectory segments, such as DLR's arc-heated LBK facilities.

Two examples for such trajectories of generic surface-to-air (SAM) and air-to-air (AAM) missiles as shown in Figure 1, with the SAM featuring a steep flight path with high initial acceleration that reaches high Mach numbers ($M > 4$) already in rather low altitudes. The AAM overall has a much longer flight duration (almost 120 s compared to just over 30 s for the SAM) including a long cruise phase at high Mach number before attacking a target at a lower altitude in the endgame.

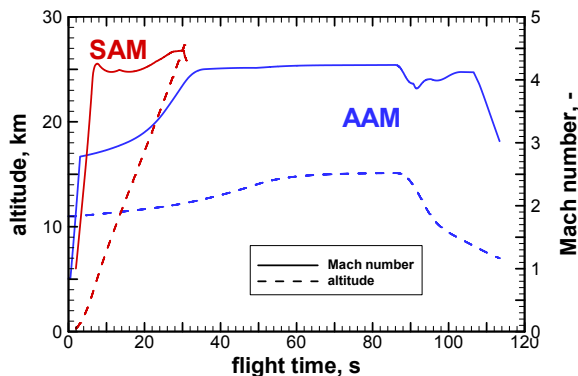


Figure 1: Sample trajectories

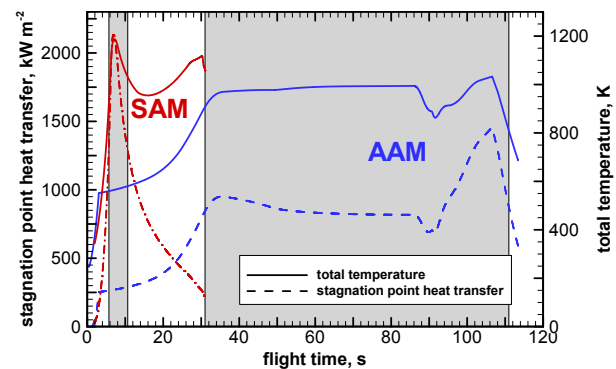


Figure 2: Stagnation point heat flux and total temperatures of sample trajectories

Figure 2 shows the total temperature and stagnation point heat loads according to the correlation by Fay and Riddell [11] that occur during these trajectories. As the diagram shows, the SAM reaches very high total temperatures of almost 1,200 K and a maximum heat flux of more than $\dot{q} = 2.1 \text{ MW m}^{-2}$ during the acceleration phase, but only for a short time. When the missile reaches higher altitudes and density decreases, the heat flux quickly becomes less. For the AAM, the heat load is rather moderate and constant during the cruise phase before it increases significantly when the missile moves to lower altitudes for the endgame.

From these trajectories, flight relevant heat loads for the replication in the arc heated facility L2K are derived by averaging the stagnation point heat loads over the time span with severe thermal loading (grey areas in Figure 2. For the SAM, this yields a heat flux of $\dot{q} = 1800 \text{ kW m}^{-2}$ for 5 seconds and $\dot{q} = 940 \text{ kW m}^{-2}$ for 80 s for the AAM (see section 2.1.2 for detailed test conditions).

Testing for the present investigation included L2K-experiments of a pure WHIPOX radome (without insulation) and VMK windtunnel tests with both OXIPOL and WHIPOX radomes. For the latter, thermal insulation has been examined as well. In both VMK and L2K testing, the temperature distribution on the exterior radome surface is measured by infrared thermography. The temperature distribution on the interior wall (for configurations without insulation) and the heating of a seeker head demonstrator are measured by thermocouples. Details on windtunnel models and measurement technologies are given in sections 2.2 and 2.3.

2. Experimental setup

2.1 Experimental facilities and test conditions

2.1.1 Vertical test section Cologne (VMK)

The vertical test section Cologne (VMK) is a blowdown windtunnel for subsonic and supersonic Mach numbers. It is capable of simulating direct flight conditions in the supersonic regime. Operating limits of VMK are Mach 2.8 at sea level, and Mach 3 and 3.2 in altitudes of 4.5 km and 7 km, respectively [12]. An overview of the VMK windtunnel is shown in Fig. 3 and the map of its operation range in Fig. 4.

The air from pressure reservoirs goes through a heat storage underneath the test chamber, where it is heated to the desired total temperature and then directed upwards through axisymmetric, contoured nozzles into the test section, which is at ambient pressure. Depending on the Mach number, different nozzle sizes are available. For the condition used in the current investigation, a nozzle with an exit diameter of 300 mm was used. Testing for the present investigation was conducted at test condition VMK-1 which is listed in Table 1 and corresponds to a flight condition of $Ma = 3$ in 4.5 km altitude. The test duration was 30 s.

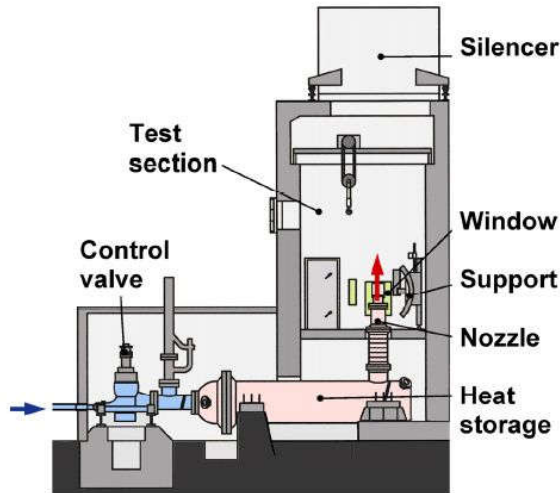


Figure 3: Schematic display of VMK windtunnel facility

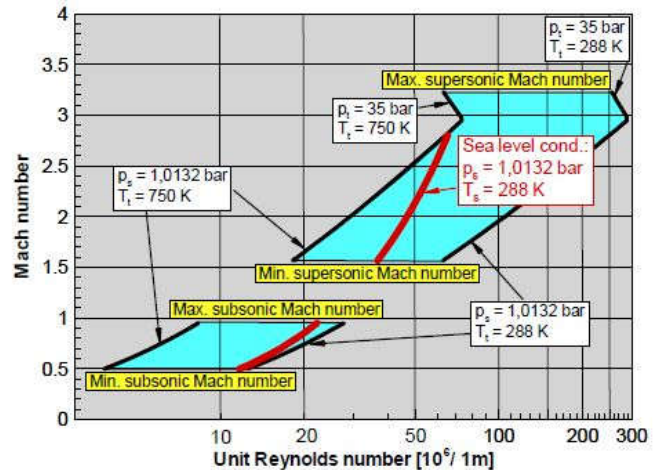


Figure 4: Operational range of VMK

Table 1: VMK test conditions

Test condition	VMK-1
Mach number	3
total pressure p_{t0} , MPa	2.1
total temperature T_{t0} , K	700
unit Reynolds number $Re_{m,\infty}$, 10^6 m^{-1}	47.4
test duration, s	30

2.1.2 Arc-heated windtunnel L2K

The arc-heated LBK windtunnel facilities of DLR Cologne are comprised of two legs, L2K for moderate and L3K for high enthalpy flows. An overview of the LBK windtunnel facility is shown in Figure 5.

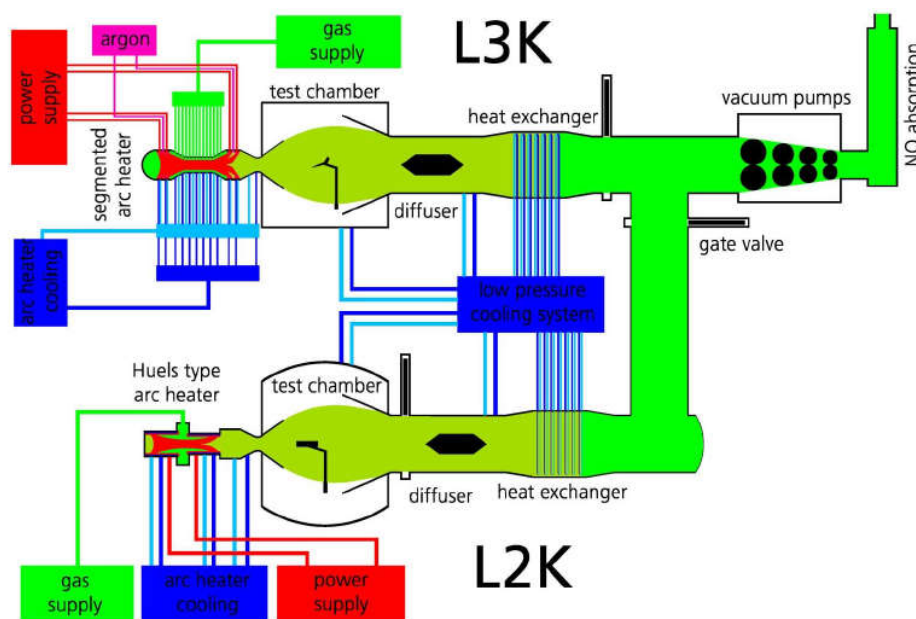


Figure 5: Arc-heated windtunnel facilities of DLR Cologne

Both legs share a common vacuum pumping and exhaust-gas cleaning (NO absorption) system. The vacuum system with five mechanical pumps allows pressure below 1 hPa. The working gases are supplied from either a storage tank with a volume 200 m³ and pressure up to 6 MPa or K-bottles with 12 m³ and 15 MPa.

The L2K facility features a Huels-type arc heater with a maximum electrical power of 1.4 MW which allows achieving moderate specific enthalpies up to 10 MJ/kg at a gas mass flow rate of 50 g/s, which corresponds to a reservoir pressure of 150 kPa. This allows for cold wall heat fluxes in air flow up to 4 MW/m². L3K has a segmented arc-heater with up to 6 MW power. It can achieve high specific enthalpies beyond 20 MJ/kg at gas mass flow rates of 100 g/s, which enables cold wall heat fluxes of 15 MW/m². Hypersonic free stream velocities are provided by a convergent- divergent nozzle. The divergent part is conical with a half angle of 12°. Different throat and exit diameters are available for variation of nozzle area ratios and thus enable Mach numbers from 3 – 10. The test conditions listed in Table 2 were chosen according to the stagnation point heat transfer rates determined from the sample trajectories and were verified by test runs with gardon gages prior to the testing campaign. Air was used as the working gas for most tests, but nitrogen was used for tests to check on the influence of surface catalycity. A more detailed description of the test facility is given by Gülhan et al. [13] or Gülhan and Esser [14].

Table 2: L2K test conditions

Huels	L2K-1	L2K-2
mass flow \dot{m} , g s ⁻¹	110	110
ratio of cold/hot gas g s ⁻¹	50/60	60/50
reservoir pressure, kPa	200	236
total enthalpy h_{t0} , MJ kg ⁻¹	2.6	3.8
reservoir temperature T_{t0} , K	2193	2905
nozzle throat/exit diameter, mm	29/50	29/50
distance from nozzle exit, mm	220	120
Pitot pressure, p_{Pitot} , hPa	89	136
heat flux \dot{q} , kW m ⁻²	940	1800
test duration t , s	80	5

2.2 Windtunnel models

The radome geometry is shown in Figure 6. It has a slender ogive shape with a very small nose radius transitioning into a much larger radius for the main part of the radome that merges into a cylinder at its downstream end. At the nose section, the wall thickness is higher due to the manufacturing processes of the CMC radomes. For the WHIPOX radome with the first model concept for the L2K tests, and the OXIPOL radome of the first VMK tests, the thickness in the nose area was about 16.5 mm (dashed line). Improvements in the manufacturing process enabled reducing the wall thickness at the tip of the radome to around 7.5 mm for the WHIPOX radomes used in VMK testing. The OXIPOL radome had an additional 30 mm long cylindrical section as elongation of the ogive curve (dashed line), while the WHIPOX radomes are finished at the end of the ogive (i.e. at 200 mm).

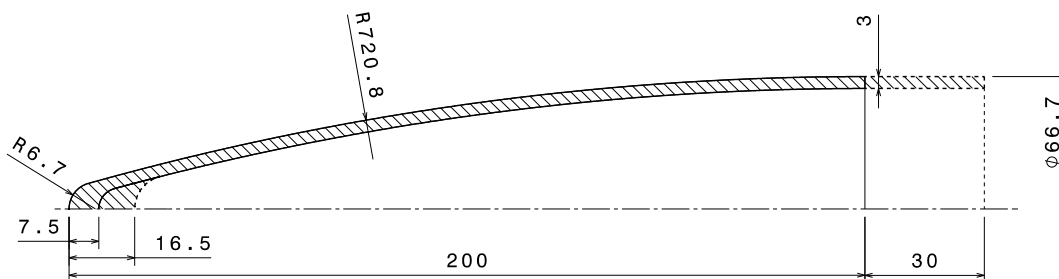


Figure 6: Radome geometry

In the experiments, two different model concepts have been used. The first configuration, shown in Figure 7 features a solid titanium core with guidance holes for 9 thermocouples that are integrated to measure the temperature distribution on the interior wall. A fastening insert is glued into the radome and a second insert is used to fixate the thermocouples' guidance core and to mount the whole model to the windtunnel support. This model concept was used for L2K testing of a WHIPOX radome and VMK testing of an OXIPOL radome. To ensure that thermocouples are in a fixed position and have good contact to the wall, a special mechanism with springs was applied. This was verified by analysing the windtunnel model with the thermocouples integrated by computer tomography, as shown in Figure 8 for a WHIPOX radome.

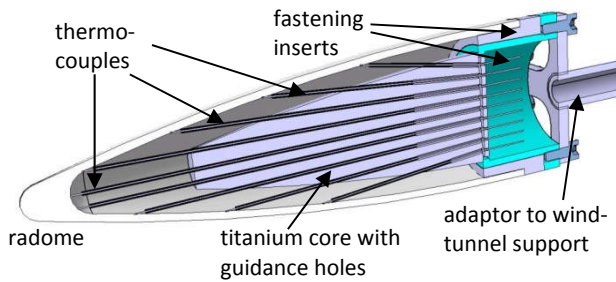


Figure 7: Cut-view of windtunnel model

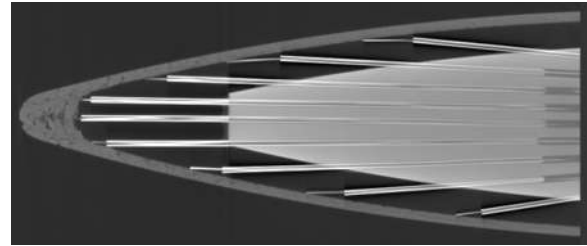


Figure 8: Computer tomography image of a WHIPOX radome with integrated thermocouples

The second model concept is shown in Figure 6. It features a seeker head demonstrator instead of the metal core in order to not only characterize the thermal behaviour of the CMC material but also to analyse its insulation capabilities by measuring the heating of the seeker head. The image on the left displays the configuration without thermal insulation. It has a guidance body for thermocouples to measure the interior wall temperature distribution of the radome in the same locations as with the first model concept. The integration of the radome hull with the seeker head and fixation to the windtunnel support is achieved similarly to the first concept with two fastening inserts. The seeker demonstrator consists of several solid aluminium parts to represent the different components of the seeker head, i.e. main body/gimbal system, antenna reflector and wave guide. The image in the right shows the configuration with thermal insulation. For this, the guidance body and wall thermocouples are removed and the tip of the radome is filled with insulator which is closed by a lid made from the same CMC material as the radome. Please note that the cutting plane in the right image is perpendicular to the one on the left in order to show the thermocouples that are integrated in this plane into the seeker head. These thermocouples are also present in the configuration without thermal insulation.

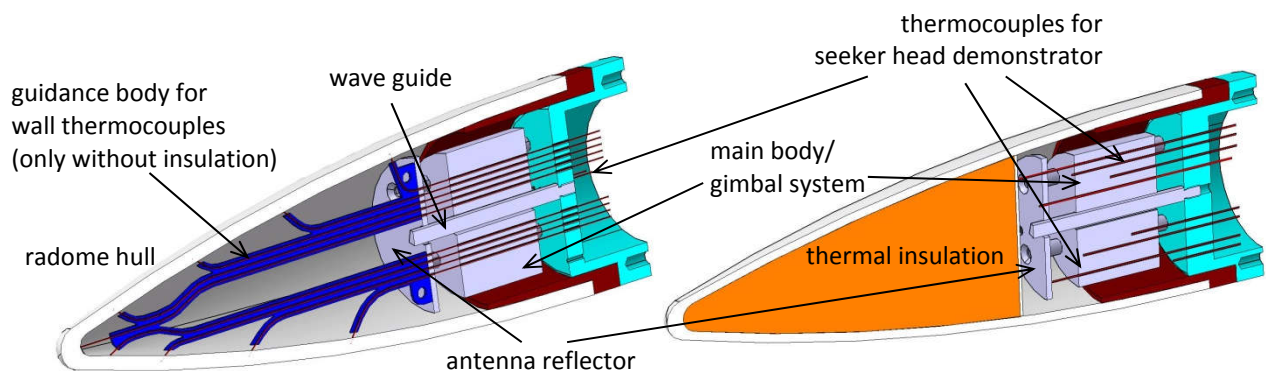


Figure 9: Cross-section views of radome model with seeker head demonstrator. Left: without thermal insulation and wall thermocouples. Right: with thermal insulation

For the tests with the second model concept, four configurations regarding the thermal insulation have been tested:

1. No insulation
2. Silica aerogel and glass fibre felt
3. Silica aerogel granulate
4. Silica aerogel with aluminium oxide (Al_2O_3)

Figure 10 shows photographs of the seeker head demonstrator with the guidance body and thermocouples for wall temperature measurements and a fully integrated radome mounted in the test chamber of VMK above the nozzle.

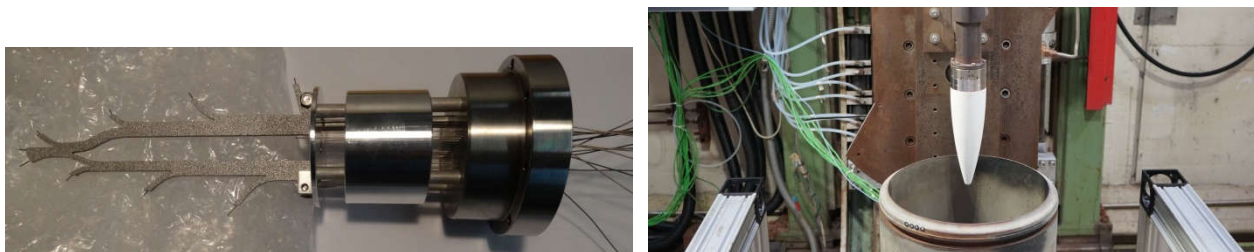


Figure 10: Seeker head with wall temperature thermocouples for configuration 1 (left) and fully integrated model in VMK test chamber

2.3 Measurement techniques

As already mentioned, 9 thermocouples (TC W1 – W9) were used to measure the temperature distribution on the interior wall in L2K-testing with the first model concept and for VMK windtunnel runs with the configuration without thermal insulation. For both model concepts, the measurement locations at the wall have been identical. They are displayed in Figure 11. For better presentation of the results, a circumferential coordinate s is defined, which gives the distance of each thermocouple along the circumference of the interior wall starting at the trailing edge on the upper side as indicated in Figure 11. Table 3 lists the position of each thermocouple. Type K thermocouples with a sensitivity of 0.75% are used.

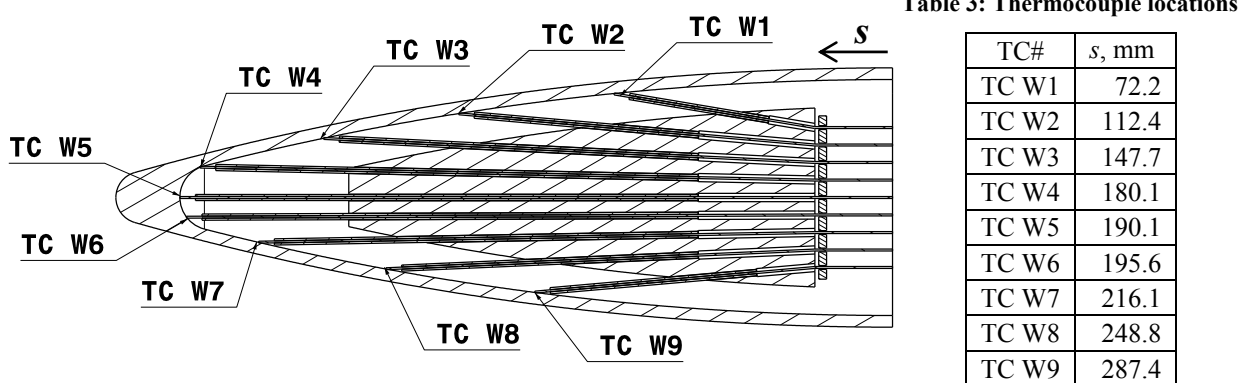


Figure 11: Distribution of thermocouples along interior wall

For the second model concept with the seeker header demonstrator, an additional 8 thermocouples, TC S1 – S8, are integrated at various spots within the parts of the seeker head and in the surrounding area. These are shown in Figure 12. The locations of the thermocouples are the same for the configurations with and without thermal insulation.

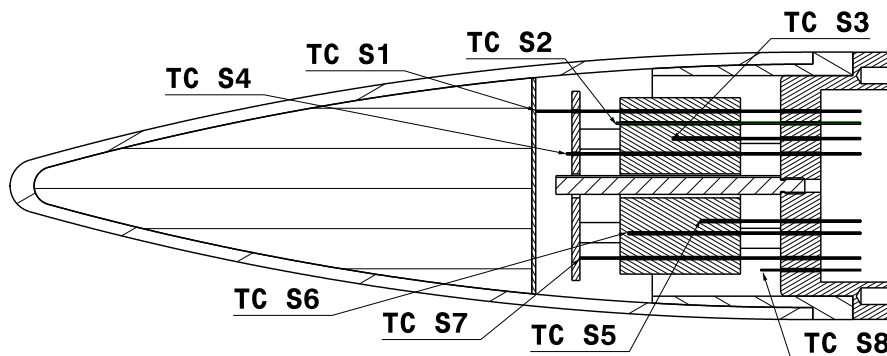


Figure 12: Positions of thermocouples in and around the seeker head demonstrator

In addition to the thermocouple measurements, the surface temperature of the exterior wall is measured with an infrared camera. In VMK windtunnel experiments, an InfraTec IR8300 with a spectral range from 2 – 5.7 μm and $\pm 1\%$ accuracy [15] was used with the OXIPOL radome and a FLIR Systems ThermaCAM SC3000 [16] with 8 – 9 μm spectral range and accuracies of $\pm 1\%$ up to 150 $^{\circ}\text{C}$ and $+2\%$ above 150 $^{\circ}\text{C}$ for the WHIPOX radome. For L2K testing, an Agema Thermovision 570 with 7.5 – 13 μm spectral range and $\pm 2\%$ accuracy [17] was used. Two two-colour pyrometers were used in L2K tests as well to measure the surface temperature close to the stagnation area.

3. Results

3.1 L2K experiments

In the investigations in the arc-heated windtunnel L2K, a WHIPOX radome with the first model concept (see Figure 11 above) for the measurement of the interior wall temperature distribution was tested. The behaviour of the material at the two different test conditions L2K-1 and L2K-2, the influence of the angle of attack and the windtunnel working gas were examined. In the experiments, the model is mounted to a movable model holder which is placed outside of the flow during the windtunnel start-up process. When the desired flow condition is reached, the model is shifted into the flow and kept there for the specified test duration. The model is then moved out of the flow before

the windtunnel is shut down, and moved back into its place to observe the cooling phase as well. The measurement data is also still recorded during this phase.

Figure 13 shows infrared images of the surface temperature distribution on the exterior wall of the radome for both conditions at the end of their respective testing times. At condition L2K-1 with a lower heat flux but higher integral heat load due to the longer testing time, the temperatures overall are much higher than for condition L2K-2. At both conditions strong temperature gradients develop with the stagnation region become much hotter than the downstream parts of the radome. Especially downstream off the point where the small nose radius transitions into the larger radius of the ogive, temperatures decline very fast.

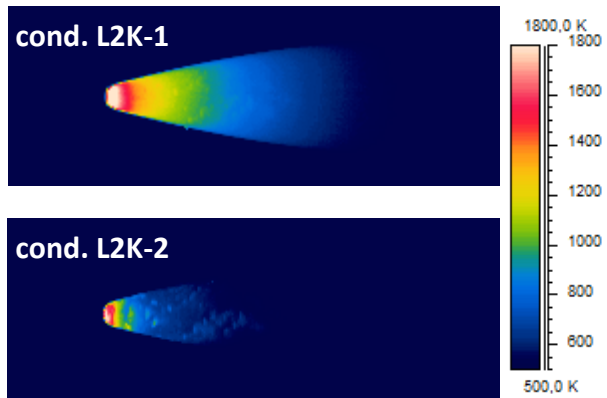


Figure 13: External surface temperature distributions from IR-thermography for both conditions

Figure 14 shows the comparison of thermocouple and pyrometer measurements for the two conditions. In the graph on the left, the timewise temperature profiles of a pyrometer aimed at a position close to the stagnation point and the three thermocouples TC W4, TC W5 and TC W6 are displayed. For better clarity and comparability the thermocouple measurements are displayed as temperature ratios normalized by their respective temperature at the start of the test run T_0 (not the total temperature of the flow). The graph shows that the material response for both conditions is very similar. On the external surface, the pyrometer measurement shows a jump of the wall temperature to over 1300 K immediately when the model is moved into the flow. For condition L2K-2, a very steep temperature rise continues to a maximum temperature of around 1560 K, while at condition L2K-1 a more moderate rise and slightly lower maximum temperature of about 1525 K is observed.

Inside of the radome, the detailed view of the thermocouple measurements shows that during the short test duration of 5 s of condition L2K-2, only at thermocouple TC W4, where the wall thickness reaches its nominal value of 3 mm after the much thicker nose section, a small temperature rise is noted, which is equal for both conditions. For another 10 s, all three thermocouples show equal temperature rises for both conditions although for condition L2K-2, the windtunnel was already shut down. For condition L2K-1, for all three thermocouples, almost linear increases with very similar gradients are observed until the end of the test duration. Temperature is always highest at TC W4, followed by TC W6 which is just slightly above TC W5 in the nose on the centreline. The right graph of Figure 14, which shows the temperature distribution along the inner wall at the end of the test time, illustrates this as well. This graph also shows the behaviour already noted in Figure 13, which shows strong temperature gradients when going from the nose to both sides of the radome. Considering that at TC W1, which is at almost 40% of the distance from the rear end of the radome to the top, the temperature only reaches about 421 K, it is assumed, that the radome most likely will hardly warm up during the tests.

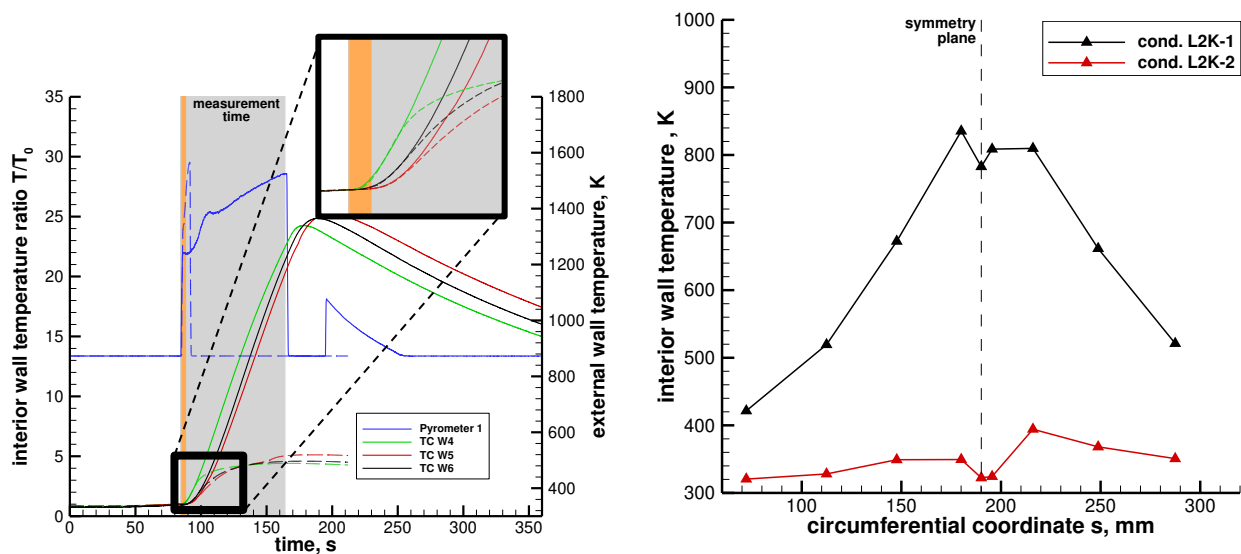


Figure 14: Comparison of temperature measurements during the test time (left) and temperature distribution on the interior wall of conditions L2K-1 and L2K-2

At condition L2K-2, it is interesting to note, that the maximum temperature is not observed around the area of TCs W4 and W6, but a bit further downstream at TC W7. Overall, the temperature increase at this condition at the interior wall is only very small, especially compared to condition L2K-1.

The influence of the angle of attack is shown in Figure 15, which shows the temperature distribution on the interior wall for $\alpha = 5^\circ$ and roll angles of $\varphi = 0^\circ$ (i.e. the plane with the thermocouples is in the x - z -plane) and 90° (thermocouples in the x - y -plane). For both conditions, the angle of attack has only small influence on the temperature distribution. As it would be expected, the temperature is decreased on the leeward and increased on the windward side. However, changes are in the magnitude of mostly $\Delta T < 20$ K, and only in some areas close to the nose, temperature differences up to 40 K are noted.

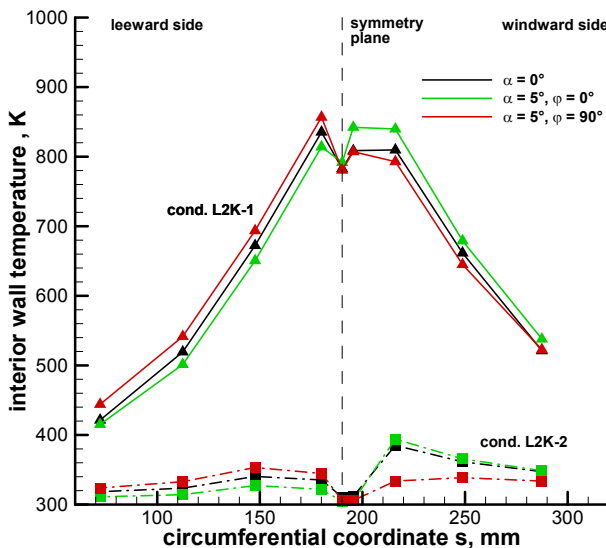


Figure 15: Impact of angle of attack in L2K tests

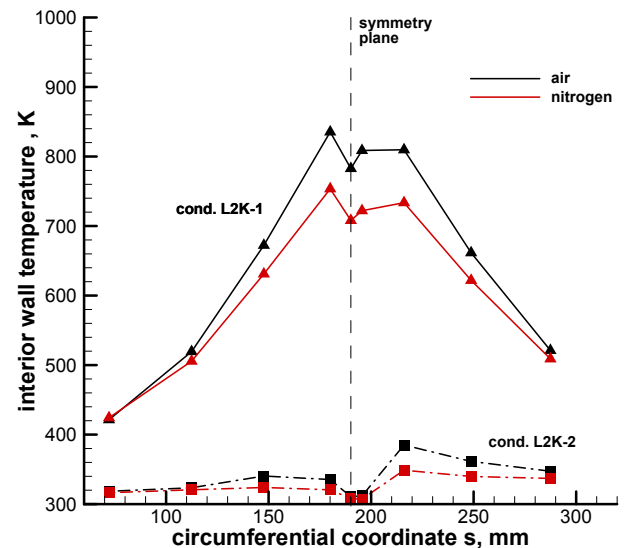


Figure 16: Impact of L2K working gas

Figure 16 shows, the impact of surface catalycity on the results by comparing test runs with air and nitrogen as test gases. As the results show, the temperatures on the inside are considerably higher in the nose section when air is used and thus higher heat loads due to catalytic reactions on the surface occur. The maximum temperature differences are over 80 K for condition L2K-1 and 30 K for L2K-2. Results clearly show that the temperature differences between the two working gases strongly increase with the surface temperature.

3.2 VMK test results

For testing in the VMK windtunnel at a Mach 3 flight condition, corresponding to an altitude of 4.5 km, an OXIPOL radome with the first model concept and WHIPOX radomes with the second model concept with a seeker head demonstrator have been used. Different to the radome geometry shown in Figure 6, the OXIPOL radome was elongated by a 30 mm cylindrical section. The ogive curve, however, was identical to the WHIPOX radomes.

3.2.1 Tests without insulation

The surface temperature distributions on the external surface of OXIPOL and WHIPOX radomes in VMK experiments, each for angles of attack of $\alpha = 0^\circ$ and 5° are shown in Figure 17. Please note that scales slightly differ as two different infrared cameras have been used for these tests. Furthermore, the viewing angle was different so that the angle of attack does not appear to be the same. For the OXIPOL radome, the IR camera was perpendicular to the plane of the angle of attack, whereas it was only 60° for WHIPOX.

Overall, the WHIPOX radome shows a more homogeneous temperature distribution on the external surface with smaller temperature gradients in flow direction (i.e. from bottom to top), whereas the OXIPOL radome heats up much more in the nose section. This is due to more solid nose part of the OXIPOL radome (see section 2.2) and the lower thermal conductivity of the OXIPOL CMC material, which inhibits the heat from being transported further downstream. Along the major part of the radome, the temperature on average is lower for OXIPOL than for WHIPOX, in the magnitude of up to 50 K (see also Figure 21). Furthermore, the spots on the surface show a more inhomogeneous distribution with temperature differences of 20 K or more in rather small spots. For WHIPOX a more gradual temperature decline in streamwise direction can be seen.

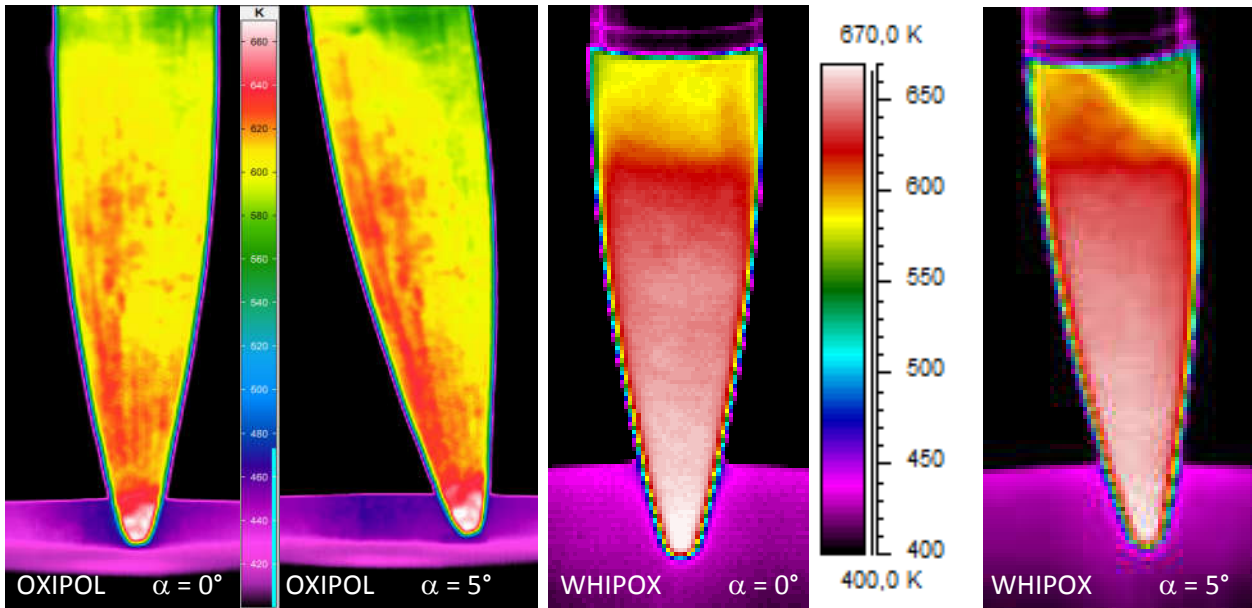


Figure 17: Infrared thermography images of VMK windtunnel tests after 30 s

The angle of attack has rather little effect on the surface temperature distribution. While for OXIPOL the windward side is notably warmer, also not very significant, hardly any difference can be noted for WHIPOX. The temperature distribution on the internal wall in Figure 18 shows this as well, with the angle of attack having no influence on the results. The temperature profiles for both materials are very different, however. For WHIPOX, the temperature in the nose tip is highest and far higher than in the rest of the radome. This can be explained by the very high heat flux in the stagnation region and the much thinner wall as compared to the OXIPOL radome, for which, similar to the L2K tests, the temperature in the nose is lower. However, as opposed to the L2K tests, in the downstream regions the radome heats up much more, so that the nose section actually shows the lowest temperature for the case without angle of attack. For $\alpha = 5^\circ$, the temperature is overall lower, with the hottest area being on the windward side a bit downstream of the nose and a gradual temperature decline on the leeward side.

In the downstream regions, temperatures on the interior wall of the WHIPOX radome are considerably lower than for OXIPOL. This is rather surprising as the exterior temperatures are higher and the higher thermal conductivity of WHIPOX would also suggest that internal wall temperatures should be higher. One reason for this behaviour could lie in the different structure of the two different model concepts as the first model concept was used for the OXIPOL and the second one for the WHIPOX radome. However, the results do not allow for any conclusion on this.

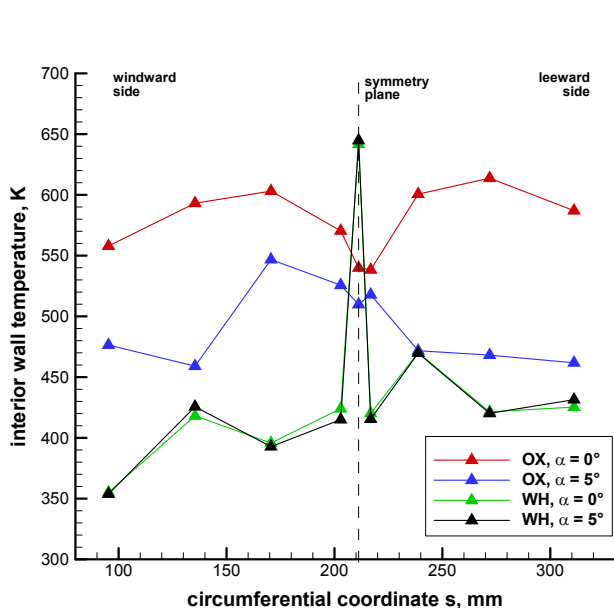


Figure 18: Temperature distribution on internal wall for OXIPOL and WHIPOX radomes

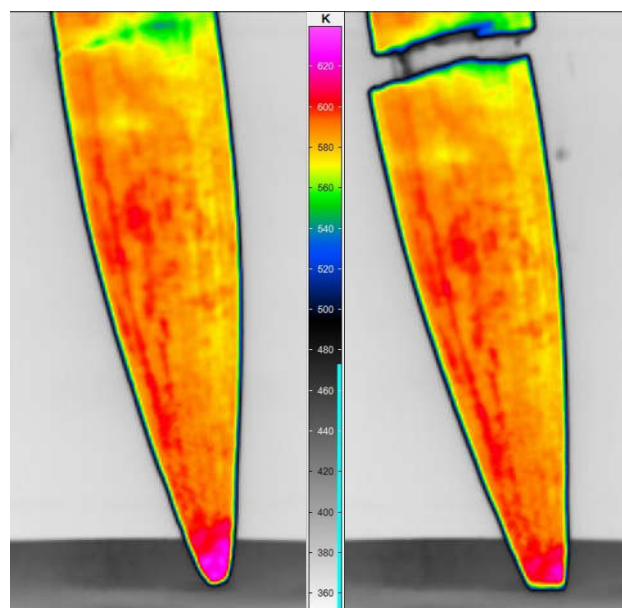


Figure 19: Collapse of OXIPOL radome during windtunnel shutdown

Unfortunately possibilities for further testing into this matter are strongly restricted as the OXIPOL radome collapsed during windtunnel shutdown of the test with $\alpha = 5^\circ$. This is displayed in Figure 19, which shows the moment just before and after the radome breaks. In the right image, the cooler region across the radome already indicated the fracture line along which the radome breaks of just a moment later. The collapse was most likely due to the combination of the model holder geometry of the first model concept, which only has a rather short fastening insert and the additional 30 mm cylindrical section at the downstream end and thus a longer lever and corresponding higher bending moment, and the significantly lower tensile strength of OXIPOL (as compared to WHIPOX by a factor of around 3). Thus, the radome was not able to withstand to strong instationary loads occurring during windtunnel shut down. However, the collapse is not thought to be linked with weakening of the material by the thermal loads as temperature dependency of the corresponding material parameters in this temperature range is rather small. It is expected that OXIPOL radomes without an additional cylindrical section and the longer fastening insert of the second model concept would survive VMK testing without problems.

3.2.2 Comparison of insulation types

Figure 20 shows the efficiency of the different insulation materials compared to the non-insulated case. The thermocouples TC S1 underneath the closing lid of the insulation, TC S6 on the bottom of the antenna reflector and TC S7 inside the main body of the seeker head demonstrator are used for this. All types of insulation work very well, i.e. they significantly lower the temperatures inside the radome around the seeker head. Aerogel granulate, which is also the most easy to handle, is far more efficient than the other two, as there already is only a very small temperature increase of less than 20 K underneath the closing lid. With less than 5 K temperature difference, the warming at the antenna reflector and inside the seeker head main body is nearly insignificant. But also the other insulation methods would lower temperatures strong enough to ensure safe operation at the tested condition.

In order to assess whether the blockage of internal heat transport by the thermal insulation has an effect on the external surface temperature, the temperature profiles along the centreline have been extracted from the infrared thermography measurements and are displayed in Figure 21, including the test with the OXIPOL radome. As the images in Figure 17 already suggested, the temperatures for OXIPOL for the major part of the radome are significantly lower. The application of any type of insulation, however, does not have any significant effect on the surface temperature. Finally, to examine the effect of the angle of attack on the heating of the seeker head demonstrator, tests with $\alpha = 5^\circ$ were performed. Figure 22 shows the results for the configuration without insulation. As can be seen, there is no noteworthy influence by the angle of attack.

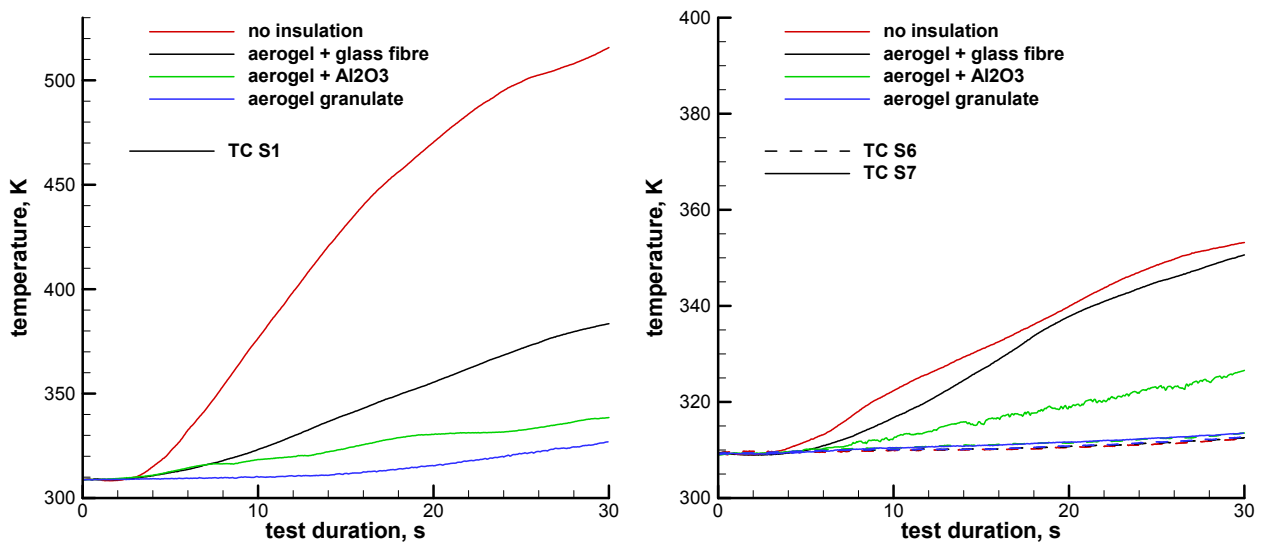


Figure 20: Comparison of efficiency of insulation materials for thermocouple S1 (left) and S6 and S7 (right)

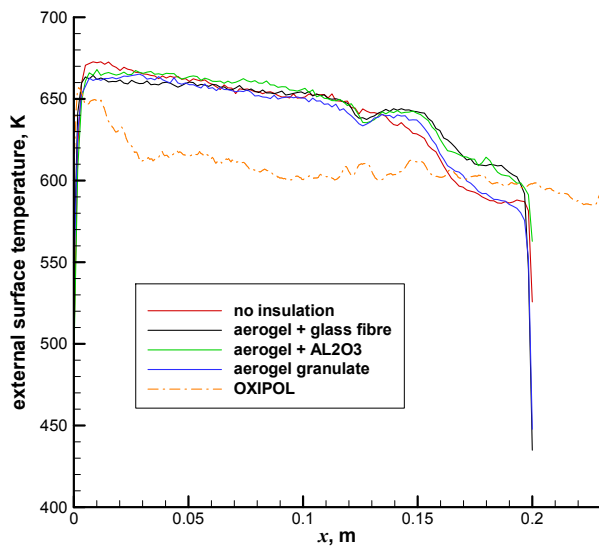


Figure 21: External surface temperature profiles along radome centrelines

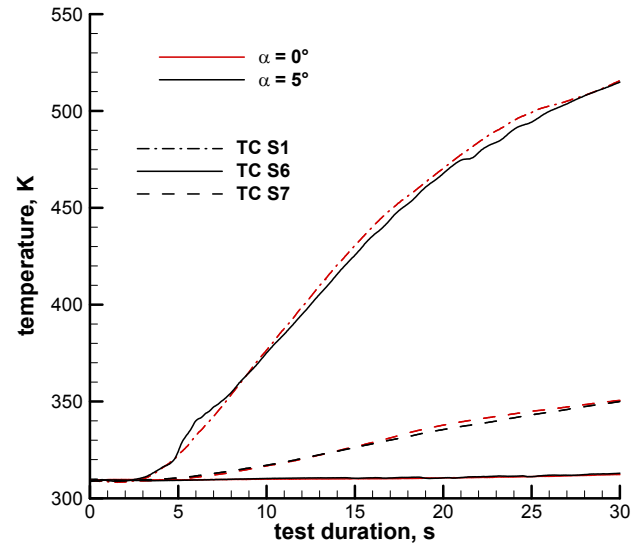


Figure 22: Angle of attack influence on heating of seeker head demonstrator

4. Conclusion

Several experimental campaigns in two different windtunnel facilities were conducted to assess the qualification of WHIPOX and OXIPOL radomes for high speed missiles. The results showed that both materials are well suitable for the thermal loads that would be expected in different mission scenarios. Although the OXIPOL radome collapsed during an angle of attack test run, it is expected that this material would be suitable as the fracture of the radome was caused by a combination of unfortunate circumstances. The WHIPOX radomes proofed suitable also for the flight relevant heat loads applied in testing in an arc-heated facility and the corresponding high temperatures. Structural integrity was not an issue for this material in any of the tests.

In addition to tests of the radome hull, different ways of thermal insulation on the basis of silica aerogels have been tested under Mach 3 flight conditions by analysing the heating of a seeker head demonstrator. All three types of insulation proved to be highly efficient with filling the radome nose with an aerogel granulate and closing it with a lid as the way with the highest temperature reduction. This method is also easiest regarding the application as it does not require a time-consuming process of coating the interior radome surface with the different aerogels.

Further testing is planned to assess the efficiency of the insulation techniques in the arc-heated L2K windtunnel for the higher temperature occurring with flight relevant heat loads. New OXIPOL radomes are also supposed to be tested with the second model concept and with thermal insulation in both VMK and L2K windtunnels to further assess the different materials and expand the technical database.

References

- [1] Göring, J., Hackemann, S., and Kanka, B., WHIPOX: Ein Faserverstärkter Oxidkeramischer Werkstoff für Hochtemperatur-Langzeitanwendungen (WHIPOX: A fiber-reinforced oxide-ceramic matrix composite for long-term high-temperature applications), *Materialwissenschaft und Werkstofftechnik*, Vol. 38, No. 9, 2007, pp. 766–772.
- [2] Schmücker, M., Grafmüller, A., and Schneider, H., Mesostructure of WHIPOX all oxide CMCs, *Composites Part A: Applied Science and Manufacturing*, Vol. 34, 2003, pp. 613–622.
- [3] Schmücker, M. and Schneider, H., *WHIPOX All Oxide Ceramic Matrix Composites*, chap. 17, Kluwer Academic Publishers, Boston, MA, USA, 2005, pp. 423–435.
- [4] Schmücker, M., Faserverstärkte oxidkeramische Werkstoffe (Oxide ceramic matrix composites), *Materialwissenschaft und Werkstofftechnik*, Vol. 38, No. 9, Sep. 2007, pp. 698–704.
- [5] Frieß, M., Göring, J., and Kemptner, E., Radomes for High Velocity Missiles Based on Oxidic CMC-Materials, *NATO RTO Symposium on Innovative Missile Systems RTO AVT-135*, Amsterdam, The Netherlands, May 2006.
- [6] Frieß, M., Heidenreich, B., and Krenkel, W., Langfaserverstärkte oxidkeramische Verbundwerkstoffe nach dem LPI-Verfahren (Long-Fibre Reinforced Oxide Ceramic Composites via the LPI process), *14. Symposium: Verbundwerkstoffe und Werkstoffverbunde*, Vienna, Austria, July 2003.

-
- [7] Frieß, M. and Denis, S., Oxide CMC Components Manufactured via PIP Processing Based on Polysiloxanes, *ECerS XII, 12th Conference of the European Ceramic Society*, European Ceramic Society, Stockholm, June 2011.
- [8] Denis, S., Frieß, M., Klatt, E., and Heidenreich, B., Manufacture and Characterisation of OXIPOL Based on Different Oxide Fibres, *High Temperature Ceramic Materials and Composites HTCMC 7*, Bayreuth, Germany, 2010, pp. 414–419.
- [9] Mechnich, P., Braue, W., Schneider, H., Koch, U., Esser, B., and Gülhan, A., Thermal Response of WHIPOX-Type All Oxide Ceramic Matrix Composites During Reentry Simulation in the DLR-LBK Arc-Heated Facility, *Proceedings of the 5th European Symposium on Aerothermodynamics for Space Vehicles*, ESA SP-563, Cologne, Germany, Nov. 2005.
- [10] Kuhn, M., Esser, B., Gülhan, A., Dalenbring, M., and Cavagna, L., Investigations on the thermal behaviour of CMC-based leading edges in hypersonic arc jet flows, *CEAS Space Journal*, Vol. 3, No. 1-2, April 2012, pp. 61–76.
- [11] Fay, J. A. and Riddell, F. R., Theory of Stagnation Point Heat Transfer in Dissociated Air, *Journal of the Aeronautical Sciences*, Vol. 25, No. 2, Feb. 1958, pp. 73–121.
- [12] Triesch, K. and Krohn, E.-O., The Vertical Test Section (VMK) at DFVLR in Koeln-Porz (Status 1986), Technical Translation ESA-TT-1053, European Space Agency, June 1987, Translation of DFVLR-Mitt-86-22.
- [13] Gülhan, A., Esser, B., Koch, U., and Hannemann, K., Mars Entry Simulation in the Arc Heated Facility L2K, *Proceedings of the 4th European Symposium on Aerothermodynamics for Space Applications*, ESA SP-487, Capua, Italy, March 2002, pp. 665–672.
- [14] Gülhan, A. and Esser, B., *Arc-Heated Facilities as a Tool to Study Aerothermodynamic Problems of Reentry Vehicles*, Vol. 198 of *Advanced Hypersonic Test Facilities, Progress in Astronautics and Aeronautics*, Progress in Astronautics and Aeronautics 13, American Institute of Aeronautics and Astronautics, Inc., Reston, VA, USA, 2002, pp. 375–403.
- [15] InfraTec GmbH, *InfraTec Image IR8300 Data Sheet*, Dresden, Germany, 2014.
- [16] FLIR Systems, *ThermaCAM SC3000 Users Manual*, Portland, Oregon, 1999.
- [17] FLIR Systems, *AGEMA 570 Operating Manual*, 1981.